International Journal for Parasitology 56 (2026) 104719

Contents lists available at ScienceDirect

International Journal for Parasitology

journal homepage: www.elsevier.com/locate/ijpara

A dedicated deep learning workflow for automatic *Fasciola hepatica* and *Calicophoron daubneyi* egg detection using the Kubic FLOTAC microscope

Salvatore Capuozzo [a,*], Maria Paola Maurelli [b], Stefano Marrone [a], Biase Celano [c], Giuseppe Martone [d], Paola Vitiello [b], Ines Hammami [b], Antonio Bosco [b], Lavinia Ciuca [b], Giuseppe Cringoli [b], Carlo Sansone [a], Laura Rinaldi [b]

[a] Department of Electrical Engineering and Information Technologies, University of Naples Federico II, Via Claudio 21, 80125, Naples, Italy
[b] Department of Veterinary Medicine and Animal Production, University of Naples Federico II, Via Federico Delpino 1, 80137, Naples, Italy
[c] Officina Elettronica SPA, Via Diocleziano 107, 80125, Naples, Italy
[d] Faculty of Technological and Innovation Sciences, Universitas Mercatorum, Piazza Mattei 10, 00186, Rome, Italy

ARTICLE INFO

Article history:
Received 6 June 2025
Received in revised form 14 August 2025
Accepted 15 August 2025
Available online 27 August 2025

Keywords:
Digital microscope
Fasciola hepatica
Mini-FLOTAC
Parasite eggs detection
Calicophoron daubneyi
Deep learning

ABSTRACT

Fasciola hepatica and *Calicophoron daubneyi* are trematodes with significant health and economic impacts on ruminant livestock farms. An effective and reliable diagnosis is essential to control their spread. To improve copromicroscopic diagnosis, the Kubic FLOTAC Microscope (KFM), a portable digital microscope, was designed for both laboratory and field use. It is based on the use of FLOTAC/Mini-FLOTAC techniques and combines their high sensitivity, accuracy and precision with a reliable system based on an Artificial Intelligence (AI) predictive model. It features automated parasite egg detection, powered by an integrated battery, a web interface for microscope control, and a dedicated AI server for image analysis. In this study, the system was optimized to better discriminate between the eggs of these two parasites through additional processing steps and a robust detection model. Two protocols, egg-spiked samples and naturally infected samples, were used to simulate different sample conditions, creating a dataset for model training and evaluation. A second dataset of field samples, with egg counts verified by optical microscopy, was used to assess performance. The detection performance during the evaluation of samples from both protocols was found to be satisfactory. Specifically, the average fecal egg count, obtained through the clinical report generated by the KFM system, exhibited a mean absolute error of only 8 eggs per sample. This result demonstrates that the KFM is a valuable tool for parasitological diagnosis that supports the livestock industry.

1. Introduction

Fasciola hepatica (liver fluke) and *Calicophoron daubneyi* (rumen fluke) are trematodes causing respectively fasciolosis and paramphistomosis in ruminants with a significant economic impact on farms (Hecker et al., 2024). Recently it has been estimated that fasciolosis causes a loss of €3 billion to the global cattle industry (Madsen et al., 2022), including approximately €750 million in Europe, with the largest impact on the dairy and beef cattle industries (Charlier et al., 2020). These economic losses are: i) direct, correlated with drug costs and liver condemnation at slaughterhouses and ii) indirect, due to reduced fertility, poor growth rates, reduced production (up to 15%) and quality of milk, as well as costs for replacement stock (Hecker et al., 2024; Howell et al., 2015).

Moreover, fasciolosis is an important human food-borne zoonosis, with confirmed cases worldwide which have risen to an estimated total of 17 million (World Health Organization, 2021; Good and Scherbak, 2023). These liver and rumen trematodes can cause different pathological conditions in animals. Fasciolosis can be present in subclinical, acute, subacute, or chronic forms. The acute and subacute forms of the disease are caused by the migration of immature parasites, which results in mechanical damage to the liver parenchyma (Adrien et al., 2013). In this phase, the main clinical manifestations are: painful distended abdomen with palpable enlargement of liver, anemic mucous membrane, reduced grazing activity (Mitchell, 2002; Lalor et al., 2021;

* Corresponding author.
E-mail addresses: salvatore.capuozzo@unina.it (S. Capuozzo), mariapaola.maurelli@unina.it (M.P. Maurelli), stefano.marrone@unina.it (S. Marrone), celano@officinaelettronica.it (B. Celano), giuseppe.martone_9149@studenti.unimercatorum.it (G. Martone), paola.vitiello5@studenti.unina.it (P. Vitiello), ineshammami4421@gmail.com (I. Hammami), antonio.bosco@unina.it (A. Bosco), lavinia.ciuca@unina.it (L. Ciuca), giuseppe.cringoli@unina.it (G. Cringoli), carlosan@unina.it (C. Sansone), laura.rinaldi@unina.it (L. Rinaldi).

https://doi.org/10.1016/j.ijpara.2025.08.007
0020-7519/

Priddle et al., 2025). Chronic fasciolosis develops when adult parasites migrate into the bile ducts and cause anemia due to hematophagy, jaw oedema, cholangitis, and fibrosis (Lalor et al., 2021). In this phase also submandibular oedema, weight loss, production losses and even death may occur. The symptoms of fasciolosis are more evident in sheep, while in cattle, clinical signs are often subclinical, such as reduced productivity and fertility, alongside decreased milk yield (Mitchell, 2002; Lalor et al., 2021; Priddle et al., 2025).

In contrast to fasciolosis, paramphistomosis is considered a less severe disease, but in recent years cases in Europe have increased and it has become one of the most important diseases of ruminants (Iglesias-Piñeiro et al., 2016).

Meanwhile, *C. daubneyi* infection causes diarrhea, cachexia, and dehydration due to the effect of the parasite on the ruminal mucosa, which negatively impacts animal production (Atcheson et al., 2022; Hecker et al., 2024). An accurate, sensitive and specific diagnosis is very important to control these trematodes and related diseases (Sabatini et al., 2023). The presence of these parasites can be confirmed by *post-mortem* at the slaughterhouse through evaluation of the upper digestive tract for rumen trematodes (Forstmaier et al., 2021), visual assessment of the liver, palpation and incision of the bile ducts and gall bladder in cases of *F. hepatica* infection (Hanley et al., 2020). On the other hand, *ante-mortem* diagnosis by immunological approaches is determined by detection of antibodies and antigens in milk, serum, plasma, feces and meat juice (Hafizah et al., 2023).

Several Enzyme Linked Immunosorbent Assay (ELISA) commercial and home-made kits (Munita et al., 2019) with high sensitivity (SN) and specificity (SP) have been developed for the diagnosis of fasciolosis (Takeuchi-Storm et al., 2017) in serum (SN 79–95%, SP 80–93%), in milk (SN 92%, SP 88%), and in feces (SN 40–98%, SP 92–94%) (Charlier et al., 2008; Howell and Williams, 2020), while some home-made ELISA have been developed to assess infection with paramphistomosis in serum (SN 86–98%, SP 24–100%) and feces (SN 8–97%, SP 88–100%) (Anuracpreeda et al., 2017; Gordon et al., 2013). However, home-made ELISA kits are sometimes difficult to reproduce in other laboratories (Calvani et al., 2018). Different molecular methods are currently available, such as polymerase chain reaction (PCR) end-point, real-time PCR, and Loop-mediated isothermal amplification (LAMP) for trematodes diagnosis, which can detect very low amounts of *F. hepatica*(Amiri et al., 2021; Calvani et al., 2018) and *C. daubneyi*(Mitchell et al., 2021; Hecker et al., 2024) DNA from feces. Despite being sensitive and accurate these techniques are costly (Mitchell et al., 2021; Calvani et al., 2018).

The laboratory diagnosis of both trematodes is currently mainly based on copromicroscopic techniques using sedimentation (Mage et al., 2002) or flotation procedures (Sabatini et al., 2023). These techniques are easy and cheap, but their main limitation lies in the variation in sensitivity and specificity among the protocols used (Reigate et al., 2021; Bosco et al., 2023).

One of the most used method is the FlukeFinder (FF), a device for egg detection and quantification based on modified sedimentation and fine filtration (Dixon and Wescott, 1987; Kurnianto et al., 2022). Recently, in a study by Hecker et al. (Hecker et al., 2024), the classical sedimentation technique and the FF technique showed similar detection rates (SN 43–65%, SP 90–100%) for both trematodes, while in another study by Kahl et al. (Kahl et al., 2023) at low level of infection (<10 EPG) FF showed a higher SN (100%) and SP (100%) compared to traditional sedimentation (SN 98%, SP 100%).

Instead, flotation procedures to identify rumen and liver fluke infections involve the use of flotation solutions with a high specific gravity (SG = 1.35) which causes egg rupture, resulting in the appearance of eggshells (Cringoli et al., 2010; Rinaldi et al., 2015). Therefore, the morphological similarity between the eggshells of *C. daubneyi* and *F. hepatica* may lead to misdiagnosis (Barrett, 2013).

In Bosco et al. (2023), the Mini-FLOTAC technique proved more accurate in estimating the intensity of *F. hepatica* and *C. daubneyi* infections at moderate and high levels than sedimentation and FF, making it potentially useful in endemic areas.

The FLOTAC and Mini-FLOTAC tools can also be used in combination with the new Kubic FLOTAC Microscope (KFM). Preliminary results obtained for the gastrointestinal nematodes showed that it is very promising for parasites diagnosis in lab and directly on field (Cringoli et al., 2021), and its automation could be very useful for accelerating parasitological diagnosis, as reported by Capuozzo et al. (2024).

Several systems for the automated detection of helminth eggs have already been described in literature, as reported in Table 1. All these systems rely on the collection and analysis of images from fecal samples.

Notably, none of these systems is capable of detecting eggs of *F. hepatica* and *C. daubneyi*, except for the Naing et al. (Naing et al., 2022) system, which can recognize *F. hepatica* eggshells, but not those of *C. daubneyi*. Indeed, the slight differences between *F. hepatica* and *C. daubneyi* eggshells make accurate recognition challenging for existing systems.

On the other hand, systems adopting the Chula-ParasiteEgg-11 (Palasuwan et al., 2022) dataset rely on images where each picture contains a single, centered and well-focused egg, leading to a bias in trained models, differently from the dataset adopted in this study, where images were extracted directly from the KFM using original fecal samples. Additionally, some commercially available all-in-one solutions, such as the Parasight System (Slusarewicz et al., 2021; Castle et al., 2024) and the DAPI (Soares et al., 2024) are designed for use in parasitology labs, as they require a power cable, while others like VETSCAN IMAGYST (Nagamori et al., 2020) involve sampling techniques that require external powered devices. Moreover, the FECPAK has been recently enhanced with an AI framework, becoming FECPAK G2 (Tyson et al., 2020; McEvoy et al., 2024; Boelow et al., 2022; Francis and Šlapeta, 2022; Rashid et al., 2018), which enables to make automatic analysis. However, no papers describe the datasets and models adopted in some of these systems (i.e. Parasight, DAPI and FECPAK G2).

For these reasons, given the promising results obtained by Cringoli et al. (2021) for the FEC in cattle samples, the aim of this study was to integrate the KFM with an AI system based on a Deep Learning (DL) model, which enables researchers, veterinarians and farmers to perform automated analyses of fecal samples potentially positive for *F. hepatica* and *C. daubneyi* eggs. In particular, given the fecal sample preparation process made with a flotation solution and the proposed Fill-FLOTAC, eggs from both classes of parasites break, leading to the emptying of eggs and, consequently, to the presence of always only eggshells, which images from samples are stored in the available dataset.

2. Materials and methods

The present study relies on the already existing Kubic FLOTAC Microscope (Cringoli et al., 2021), enhances its firmware to make it compatible with dataset collection and automatic scan functionalities, and adds an AI system on server that communicates with the microscope, processes images from scan sessions and generates clinical reports. These functionalities are easily accessible through the web interface once the user connects to the KFM.

The improvements made to the microscope internal system include:

Table 1
Automated systems for parasite egg detection

Reference	Dataset Classes	DL Models
Rashid et al. (2018) Tyson et al. (2020) Boelow et al. (2022) McEvoy et al. (2024) (FECPAK G2)	Gastrointestinal nematodes, Equine strongyle and *Parascaris* spp.	Unspecified model
Viet et al. (2019)	*Ascaris*, *Diphyllobothrium*, *Enterobius*, Hookworm, *Metagonimus*, *Schistosoma*, *Taeniarhynchus* and *Trichuris*	Faster R-CNN
Kitvimonrat et al. (2020)	*Opisthorchis viverrini* and Minute Intestinal Flukes (Lee et al., 2012)	Faster R-CNN, RetinaNet and CenterNet
Ray et al. (2020)	*A. lumbricoides*	ANN and SVM
Nagamori et al. (2020, 2024)	*Ancylostoma* spp., *Trichuris* spp., *Toxocara* spp., *Taenia* spp., *Cystoisospora* spp., *Giardia* spp. and *Parascaris* spp.	Single Shot MultiBox Detector with Inception v2 backbone
Steuer et al. (2024) (VETSCAN IMAGYST)	*Equine strongyles*, *Parascaris equorum*, *Trichostrongylid*, *Ancylostoma* spp., *Toxocara* spp., *Trichuris* spp., and *Ascaridia galli*	Unspecified model
Slusarewicz et al. (2021) Castle et al. (2024) Cain et al. (2024) (Parasight System)		
Mayo et al. (2022)	*A. lumbricoides*, Hookworm, *O. viverrini*, *Taenia* spp. and *T. trichiura*	GAN and Faster R-CNN
Ruiz-Santaquiteria et al. (2022)	*A. lumbricoides*, *C. philippinensis*, *E. vermicularis*, *F. buski*, Hookworm, *H. diminuta*, *H. nana*, *O. viverrini*, *Paragonimus* spp., *Taenia* spp., and *T. trichiura* (Palasuwan et al., 2022)	Faster R-CNN with its variants, Task-aligned One-stage Object Detect. model and YOLOX
Pedraza et al. (2022)	*A. lumbricoides*, *F. buski*, *H. diminuta*, *Taenia* spp., and *T. trichiura* (Palasuwan et al., 2022)	Vision Transformer, Mask R-CNN, Deformable-DETR and Cascade Mask R-CNN
Wang et al. (2022)	*A. lumbricoides*, *C. philippinensis*, *E. vermicularis*, *F. buski*, Hookworm, *H. diminuta*, *H. nana*, *O. viverrini*, *Paragonimus* spp., *Taenia* spp., and *T. trichiura* (Palasuwan et al., 2022)	YOLOv5 and Cascade R-CNN
Naing et al. (2022)	6 protozoan cysts and 28 helminthic eggs (including *F. hepatica*)	YOLOv3 and YOLOv4-Tiny
Rajasekar et al. (2023) (Parasite.ai)	*A. lumbricoides*, *C. philippinensis*, *E. vermicularis*, *F. buski*, Hookworm, *H. diminuta*, *H. nana*, *O. viverrini*, *Paragonimus* spp., *Taenia* spp., and *T. trichiura* (Palasuwan et al., 2022)	YOLOv8 and Inception-v3
AlDahoul et al. (2023)	*A. lumbricoides*, *Capillaria philippinensis*, *Enterobius vermicularis*, *F. buski*, Hookworm, *H. diminuta*, *H. nana*, *O. viverrini*, *Paragonimus* spp., *Taenia* spp., and *Trichuris trichiura* (Palasuwan et al., 2022)	EfficientNet, DenseNet, Vision Transformer and CoAtNet
Kumar et al. (2023)	Hookworm, *H. nana*, *Taenia* spp., *A. lumbricoides*, and *F. buski*	YOLOv5
Suwannaphong et al. (2023)	*Ascaris lumbricoides*, *Hymenolepis diminuta*, *Fasciolopsis buski* and *Taenia* spp.	AlexNet and ResNet50
Wang et al. (2024)	*Clonorchis sinensis*, Hookworm, and *Blastocystis hominis*	YOLOv5
Xu et al. (2024)	*A. lumbricoides*, *C. philippinensis*, *E. vermicularis*, *F. buski*, Hookworm, *H. diminuta*, *H. nana*, *O. viverrini*, *Paragonimus* spp., *Taenia* spp., and *T. trichiura* (Palasuwan et al., 2022)	YAC-Net (Modified YOLOv5n)
Soares et al. (2024) (DAPI)	*A. lumbricoides*, *S. stercoralis* and *G. duodenalis*	Unspecified model
Cure-Bolt et al. (2024)	*A. lumbricoides*, *T. trichiura*, and Hookworm	AI-DP-based Kato-Katz
Ward et al. (2024,)	*Ascaris*, *Trichuris*, Hookworm and *Schistosoma mansoni*	AI-DP-based Kato-Katz 2.0

- Homing functionality: starting from any position of the tray holding the FLOTAC or Mini-FLOTAC apparatus, the KFM system automatically locates the homing position, corresponding to the upper-left corner of the analyzed floating chamber. Moreover, it adjusts the best z-position of the camera to maximize focus on the eggshells.
- Autoscan functionality: starting from the homing position, the KFM system automatically moves along the floating chamber, following a serpentine path, as illustrated in Fig. 1. In this way, it captures 192 images with a resolution of 1600x1200 covering the whole chamber (16 rows by 12 columns, with each column 1 mm wide).

Once the scan images are collected, the system starts the download process from the device connected to the KFM, retrieving a zip file containing the captured images.

As mentioned above, the KFM system is powered by a Deep Learning workflow hosted on a dedicated remote server, where the model responsible for eggshell detection is stored. However, in order to make the model capable of detecting those eggshells, a training workflow where the model was trained and optimized on a collected dataset of images and labels was required.

2.1. Training workflow

To train and validate the Convolutional Neural Network (CNN) adopted to recognize and count the eggshells of *F. hepatica* and *C. daubneyi* with KFM, five main phases were required:

- Preparation of fecal samples using the Mini-FLOTAC technique (Cringoli et al., 2017);
- Automatic scanning of fecal samples with the KFM;
- Scanning of images labeling through a dedicated labeling tool;
- Dataset collection and split of images and labels of *F. hepatica* and *C. daubneyi* eggshells for the training process;
- CNN model training and optimization.

2.1.1. Fecal sample preparation

Fecal samples were collected from naturally infected cattle with *F. hepatica* and/or *C. daubneyi* at three farms located in the Caserta, Salerno and Avellino provinces in the Campania region (southern Italy) to obtain images of the eggshells of these two trematodes.

At each farm, individual fecal samples were collected directly from the rectum of 20 cattle and analyzed using the FLOTAC basic technique which has an analytical sensitivity of 1 egg per gram

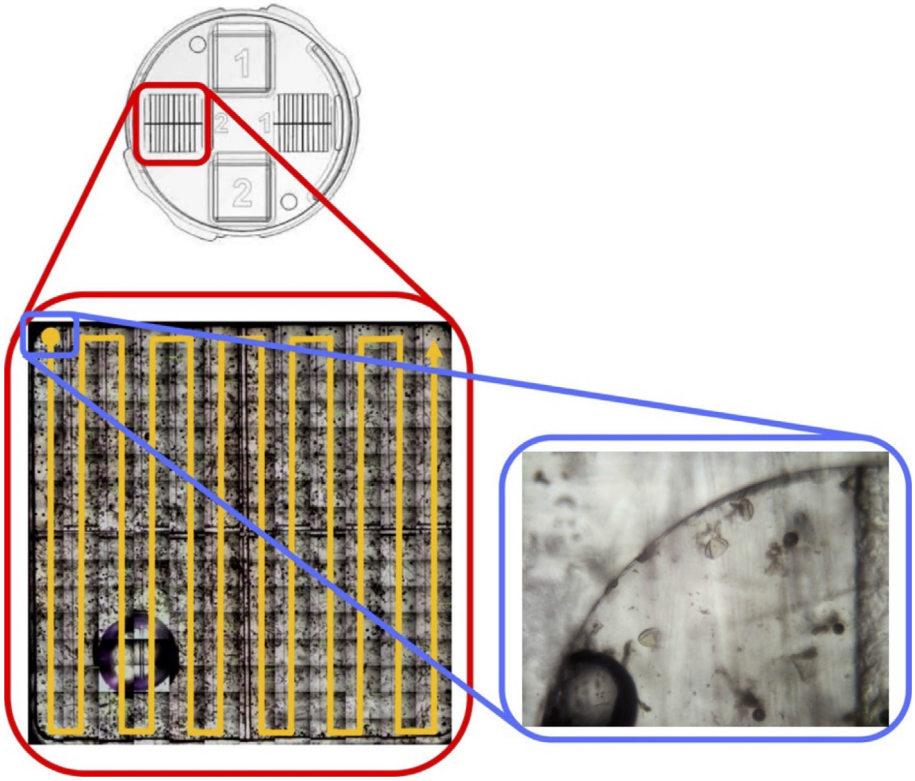

Fig. 1. Serpentine path of the autoscan process.

(EPG) of feces in three replicates. A zinc sulphate flotation solution (specific gravity = 1.35) was used to identify the positive and negative samples (Bosco et al., 2023).

To simulate different sample conditions (dirt, number of eggs, etc.), two different protocols were adopted for fecal sample preparation using the Mini-FLOTAC:

- Egg-spiked samples were prepared using negative cattle fecal samples artificially infected with *F. hepatica* or *C. daubneyi* eggs to achieve different levels of EPG, following a protocol described by Bosco et al. (2023). The extraction protocol was used to obtain mono-infected samples for each fluke egg. Four sieves of different mesh sizes ($1mm, 250\mu m, 212\mu m$ and $63\mu m$) were used to separate eggs from feces. The last $63\mu m$ sieve was washed with tap water to recover the eggs which were then sedimented in a conical beaker for 4 min. The supernatant was removed and the purified egg suspension obtained was resuspended in distilled water. To determine the concentrations, the arithmetic mean of egg counts in ten $10\mu l$ aliquots was calculated. Concentrations of 500 EPG were prepared by adding appropriate egg suspensions to negative fecal samples, ensuring approximately 50 eggshells in each chamber of the Mini-FLOTAC. This protocol kept the chambers of the apparatus clear, with minimal vegetable components, debris or foreign matter;
- Naturally positive cattle fecal samples, diluted 1:10 according to the standard diagnostic protocol were used to train the system incorporating some debris that partially covered the eggshells (Cringoli et al., 2017).

2.1.2. Automatic scan session

The latest version of the KFM firmware enabled the collection of images from prepared samples. Once several Mini-FLOTAC apparatuses were prepared, the KFM scanned them in sequence.

Depending on the protocol adopted for sample preparation, the collected scan images showed different characteristics in terms of debris and background content, as illustrated in Fig. 2.

The scan session produced the first dataset of images, which included samples obtained from both egg-spiked and naturally infected preparations. To evaluate system performance on independent data, a second dataset (external test set) was generated using naturally infected field samples with varying levels of debris.

During the external test set collection, manual counting of parasitic elements using an optical microscope was performed and compared to automated counting performed by the KFM.

2.1.3. Scan images labeling

All the zip files from the scan sessions were used to create the Trematodes AI-KFM Dataset (Capuozzo et al., 2025), a subset of the complete AI-KFM Dataset containing more than 20 classes of parasite eggs, in addition to the trematode eggshells and foreign matter.

Unlike the previous dataset collected for the AI-KFM Challenge[1], adopted by challengers as described by Capuozzo et al. (2024), this dataset contains only samples of *F. hepatica* and *C. daubneyi* eggshells, because these two classes were the main focus of this research activity.

Each image in this dataset contains at least one eggshell of either *F. hepatica* or *C. daubneyi*, and all eggs were marked and labeled with a bounding box by experts like parasitologists. This labeling process was made possible thanks to a dedicated toolkit, developed in Python from the ground up, called "KFM Tools"[2].

The criteria adopted for eggshell labeling were as follows:

[1] AI-KFM 2022 Challenge: https://sites.google.com/view/ai-kfm2022/
[2] KFMTools: https://github.com/SalvatoreCapuozzo/KFMTools/

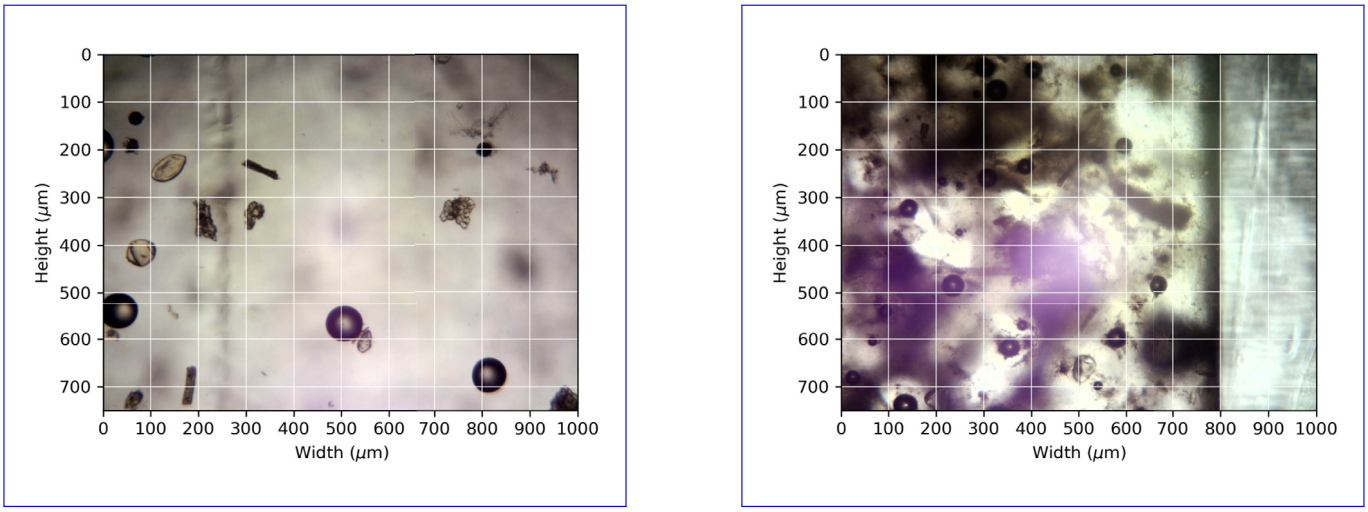

(a) Egg-spiked sample (b) Naturally infected

Fig. 2. Scan images obtained with the two different protocols. Each image corresponds to a window in the apparatus chamber of size $1000\mu m * 750\mu m$. Eggshells have an average length of $75\mu m$.

- Eggshells were labeled if recognizable by the domain expert, who is a parasitologist, regardless of the focus quality;
- eggshells were labeled if at least 50% of their shape was visible, even if compromised by foreign matter or positioned at the edges of the image;
- in every image, all the eggshells were labeled, and if labeling was not possible according to the above criteria, the image was removed.

2.1.4. Dataset collection and split

Despite these strict rules for obtaining the dataset, the number of labeled eggshells was sufficient for model training. Indeed, to train the CNN model, a portion of the Trematodes AI-KFM dataset, known as the "training set", was extracted. Another portion, the "validation set", was used to optimize model hyperparameters, such as learning rate and batch size. Finally, a third portion was adopted to evaluate the system with the dataset composed of training and validation sets once the optimal hyperparameters were obtained. The dataset splits were balanced through the sample preparation approach.

The "internal test set" was obtained by extracting 20% of the complete dataset with a hold-out approach, while the other two were obtained by performing a 5-fold cross validation on the remaining 80% share.

The reason why the test set was called "internal test set" was that more than half of the images, especially those with egg-spiked dilutions, represented an ideal condition where the chamber was clean and the eggs were easy to recognize. However, sample analysis is typically performed on dirtier samples, with chambers full of fecal matter and foreign material. Therefore, to obtain a more complete overview of performance, it was necessary to evaluate the system on another test set, called "external test set", with more realistic characteristics. In other words, two test sets were adopted:

- **Internal test set**, described above, extracted from the hold-out split of the original Trematodes AI-KFM Dataset
- **External test set**, derived from new scan sessions of naturally infected samples, performed using KFMs and a standard 1:10 dilution

For the external test set, 16 scan sessions were performed with varying random levels of debris, as would occur in a real context. This ensured that the evaluation metrics for this set provided a more realistic description of the system performances.

2.1.5. Model training and optimization

Once all the subsets were collected, it was possible to train the DL model. In particular, as remarked in the related studies, the best possible solution was to use the validated State-of-the-Art architecture for Object Detection in several domains: YOLOv8 (Redmon et al., 2016; Terven and Cordova-Esparza, 2023).

Starting from the Trematodes AI-KFM Dataset, a YOLOv8 model was trained for deployment on the AI server workflow.

The attempts made to optimize the trained model included adjustments of hyperparameters and changes in model size.

Given the server computational power and availability, there were no constraints on the model complexity and size, therefore the choice shifted toward the most accurate model, regardless of latency, which was, even in the worst case, of only few milliseconds per image.

2.2. Inference workflow

Once the optimal model was obtained, it was inserted into the AI server for the inference workflow. In this way, after the end of the autoscan process, it was possible to send the collected images with either the web interface or the dedicated tool in the KFM Tools in order to start the inference process.

Once the images were collected, the automatic detection process powered by the trained model was started and, in few seconds, it generated labels along with the parasitological report of the scan. This allowed the operator to retrieve the results of the sample analysis consisting of the eggshell count for each class, as well as their spatial detection on images, and to use labels (after a manual check) to increase the amount of images in the dataset.

As reported before, the autoscan process produced a collection of 192 images. Technically, both the server and the KFM Tools had the capability to concatenate these images properly in order to reconstruct the whole chamber. However, since image resolution was already high enough and resizing a large image of the

chamber to fit the model would make the detection subjects too small, the strategy to make predictions on all images separately was adopted.

Moreover, in addition to the detection model, a knowledge-based filter was applied, which, considering the *F. hepatica* and *C. daubneyi* parasite eggshells, always removed predictions with a bounding box area outside the range $\left[(80px)^2, (144px)^2\right]$ for an image of resolution 1600x1200. Given that the width in an image always corresponded to 1 mm, the conversion factor was 0.625 μm per pixel, therefore range values correspond to $(50\ \mu m)^2$ and $(90\ \mu m)^2$. Since, in the training dataset, no egg had an area outside this range, new detections with anomalous values could be safely discarded. This addition led to a decrease in false positives (FP).

In this way, we had a filtered collection of predictions for each image and, without further processing operations, the result would be the cumulative sum of counts for each class. However, these operations were required for two reasons:

- The neural network was not aware of changes in lighting, therefore it could misclassify eggshells having similar colors, but under different conditions;
- images from scan sessions were not completely disjointed from one another, indeed there was a slight and not precisely defined overlap at all the edges, due to technical limitations of the mechanical components of the KFM, resulting in not sensible enough tray motion steps.

For these reasons, besides the detection performed by the DL model, a pre-processing step on scan images was included before the detection, as well as an overlap-aware counting process, which occurred after the predictions on all images, and is described in detail below.

Given the heterogeneity of the training set samples and the different light conditions in the images, there was an urgency to perform some pre-processing on the available images.

Since FEC performance was not only dependent on the model itself, but also on the processing steps performed, this study illustrates the whole detection workflow, which proceeds as follows:

- Images are collected from the scan process;
- images are pre-processed and enhanced with color grading;
- the AI model detects all the eggshells on the processed images;
- the system counts the number of eggshells in chambers with an overlap-aware approach;
- starting from detection results and sample preparation info, a clinical report is generated.

In particular, the image pre-processing and color grading step, as well as the overlap-aware filtering step, will be detailed in this study.

2.2.1. Image pre-processing and color grading

The KFM hardware was originally designed to minimize external influences and to optimize image quality thanks to camera autoexposure and color correction algorithms. However, dirt and bubbles affected the appearance of images, altering the colors of eggshells in images which could lead to incorrect detections by the AI model. For instance, an overexposed *F. hepatica* eggshell might resemble *C. daubneyi*, and a *C. daubneyi* eggshell, when color-shifted with addition of red could be mistaken for *F. hepatica*.

For this reason, it was crucial to apply pre-processing techniques to the scan images to retrieve the accurate detections. In microscopy-based parasite egg detection, color grading algorithms can enhance image quality by compensating for variability introduced by inconsistent lighting conditions or staining protocols. These algorithms typically apply global transformations, such as histogram matching or color normalization in decorrelated color spaces like Lab or HSV, that standardize brightness and chromaticity across samples. Crucially, such transformations preserve the relative color ratios between different objects within the image, ensuring that diagnostically relevant chromatic cues, such as pigment concentration or structural color differences between egg types and background debris, remain intact. This enables improved consistency in visual appearance across datasets while maintaining the spectral relationships essential for robust detection and classification by both human experts and automated models.

For this specific use case, the adopted approach involved selecting a small subset of images from the training set with ideal conditions (an example of this kind of sample image is shown at the top of Fig. 3). The probability density function (PDF) of this set was computed and its average was used to perform color mapping on the input images aligning them with the reference distribution. The result was a set of images whose color palette closely matched that of the reference set. The explanation of the algorithm used for this automatic color grading can be found in Pitié et al. (2007).

Even though the dirtiness levels varied across the images, the relationship between eggshell color and the background remained consistent, meaning that a darker image resulted in proportionally darker backgrounds and eggs, and consequently their color ratio was almost identical. By applying a PDF transfer, the color relations did not change, retrieving colors similar to those in the training dataset, and enabling accurate identification by the neural network. At the bottom of Fig. 3 there is an example of color grading, showing the transformation from an original "dirty" image of a sample to its "cleaned" version.

Given this pre-processing step, the egg detector network could be trained with both the original training set and a "uniformed" version, where all the training images were converted using the described algorithm. Another hyperparameter adopted for the training process was the type of training set—original or processed.

This approach, as shown in the Results section, improved and partially resolved the issue with dirty samples. However, because multiple images were generated per scan, where a single chamber scan yielded a 16x12 matrix of images, another challenge was the occurrence of the same egg in two or more different and contiguous images, in particular near image edges. This occurred due to minor mechanical imperfections in the microscope hardware, on the order of fractions of a millimeter, and for design choices, in particular the decision to make consecutive images slightly overlapped rather than completely mutually exclusive. This was done as a safety measure to ensure no egg was missed. However, the consequence of these overlaps was the generation of eggshells duplicates, as illustrated in the next paragraph, which mislead the counting process.

2.2.2. Overlap-aware counting process

The images forming the entire floating chamber could include duplicate eggshells, caused by slightly overlapping contiguous images, which could not be identified as the same by the DL model itself since it processes input images independently. Indeed, if an eggshell at the bottom of one image reappeared at the top of the next image directly below it, the detection model would neither recognize nor account for it. However, a second algorithm operating after the DL model could address the issue.

Given a predefined delta of maximum overlap size, called Δ_o, a predefined delta for the possible eggshell shift, called Δ_s, and a

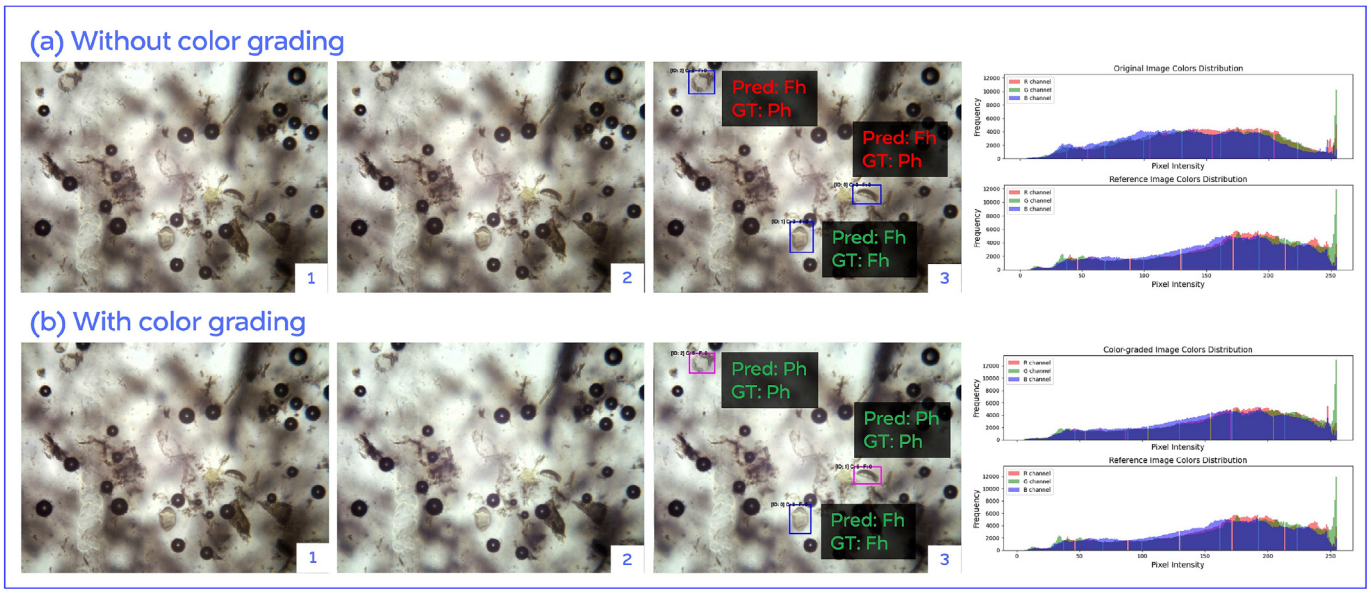

Fig. 3. Processing and inference pipelines examples on the same "dirty" image. Pipeline (a) does not apply color grading (images (a1) and (a2) are the same) and colors distributions of the image and of a reference image from the dataset the color grading is fixed on are reported on the right. Pipeline (b) apply color grading (image (b2) is the color-graded version of image (b1)) and colors distributions of the image and of the same reference image are reported on the right. (a3) and (b3) report differences on inferences brought by the color grading process.

minimum similarity index, called i_{ss}, the algorithm could extract positions of eggshells located in the bands of size Δ_o at the edges of images (in particular, bands with height Δ_o at top and bottom edges, and with width Δ_o at left and right edges). For each pair of contiguous images, the eggs extracted from the bands of the common edge were compared by their position, and their images cropped by bounding boxes were compared to check similarity.

For instance, given two images, one below the other, where the top image was called A and the bottom one B, the lower band of A and the upper band of B represented the common edge. Given an egg from band A with position (x_A, y_A) and one from band B with position (x_B, y_B), the process calculated the difference between x_A and x_B. Additionally, there was a process calculating the structural similarity index (SSIM) (Wang et al., 2004) between the two eggs inside the corresponding bounding boxes. If the difference was below Δ_s and the index was above i_{ss}, the two eggshells were considered the same and only the one from image A was counted. Fig. 4 is a visual representation of the explained example.

In case of eggshells partially appearing in one image and totally appearing in another, there was no issue, since the complete egg was outside the edge band, while the partial egg was not detected, thanks to the criteria adopted for dataset generation. Therefore only one egg was extracted, as expected.

3. Results

Performances of the KFM detection system were influenced by the dataset size, the DL detection model operating on pre-processed images and the overlap detection pipeline.

In particular, the Trematodes AI-KFM dataset was composed of 6,186 labeled eggshells for *F. hepatica* and 3,234 for *C. daubneyi*. In this dataset, images are named after the scan session ID, therefore it is possible to identify which images come from the same sample. With this information, it is possible to analyze distribution of eggshells with their mode and median values, representing respectively the most common number and the average number of eggshells, both for each scan and for each image. In particular, it is possible to state that:

- For each scan session, the distributions of the number of *F. hepatica* and *C. daubneyi* eggshells are Poisson distributions with peaks respectively of 10 and 5 eggshells per chamber, and average values respectively of 30 and 53;
- for each single image, the distributions of the number of *F. hepatica* and *C. daubneyi* eggshells are Poisson distributions with peaks respectively of 1 and 2 eggshells per chamber, and average values of respectively 2 and 5.

Consistently with the adopted sample preparation process, the result of this analysis showed that the average number of fecal eggshells (considering both egg classes) was about 40. As shown in Fig. 2, scan images with different preparation protocols had different densities of eggshells. In particular each egg-spiked image had a higher number than the average, which was 2 for *F. hepatica* and 5 for *C. daubneyi*.

The main evaluation metric adopted on the test sets was the mean average precision at 50% (mAP50), which is the average precision across all the classes with an intersection over union threshold of 0.5. Moreover, other evaluation metrics, such as precision, recall and F1-score, were adopted. Formulas for these metrics are reported below, where TP is the number of true positives, FP the number of false positives and FN the number of false negatives:

$$Precision = \frac{TP}{TP + FP} \tag{1}$$

$$Recall = \frac{TP}{TP + FN} \tag{2}$$

$$F1Score = 2\frac{Precision * Recall}{Precision + Recall} \tag{3}$$

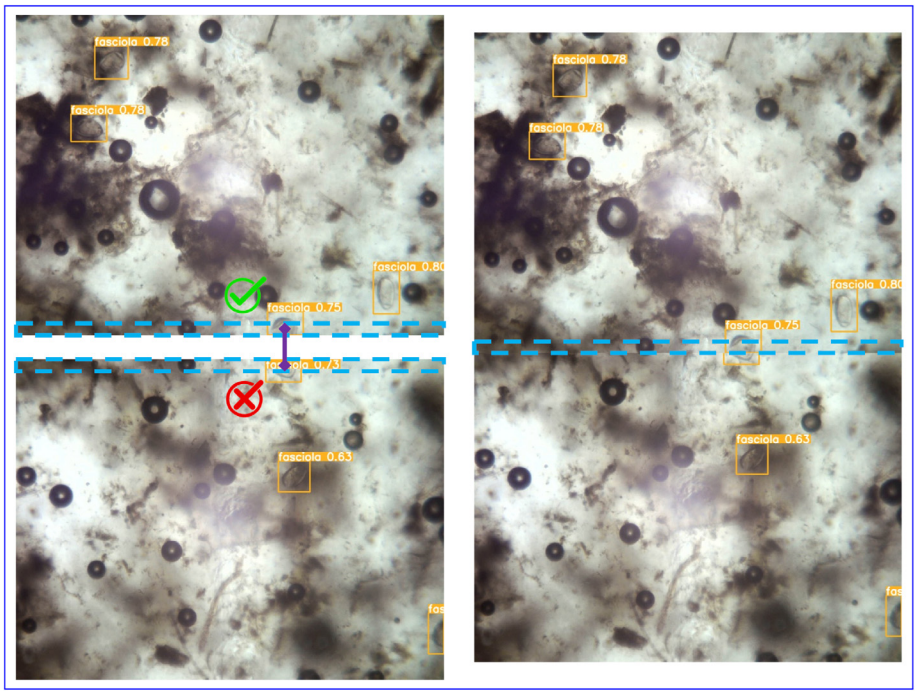

Fig. 4. Selection of the eggshells from two contiguous images.

On the other hand, since the system output was the count in samples for each egg class, the mean absolute error (MAE) was another metric adopted for system evaluation. MAE can be obtained as follows, where y_i is the i-th prediction, $\hat{y}_i$ is the i-th true value and n is the number of observations:

$$MAE = \frac{\sum_{i=1}^{n} |y_i - \hat{y}_i|}{n} \quad (4)$$

3.1. Validation of system efficacy with internal test set

In order to verify whether, in a controlled setup, the AI system performs equally well for all the available classes, a balanced test set from the available dataset has been extracted. As the original dataset, this test set contains both naturally infected and egg-spiked samples, and the classes have been sampled with a balancing approach. In this way, results obtained from this session are not biased and truly outline the efficacy of the KFM system on the available classes.

Given the hold-out split of the original dataset, models with the YOLOv8 architecture were trained with a 5-fold cross-validation approach to identify the best hyperparameters. The average results were then sorted by mAP50, obtained from inferences on the validation set. This metric was chosen at the expense of mAP95 because the focus was not on the precision of bounding boxes, but only on the correct detection of a specific class of eggshell in a certain position, and the consequent count of the eggshells in a session.

Table 2 shows the best attempts performed with different hyperparameters and model dimensions along with the average mAP50 of the five models from the cross validation.

Once chosen, the model with the best mAP50 was adopted to make inferences on the internal test set and extract results. Since the dataset was heterogeneous, the test session was performed on different data sets, where the difference was in sample dilution and eggshell extraction. Therefore, the results represented an average performance metric of the trained system.

Table 2
Model and hyperparameters best attempts with average mAP50 for every cross-validation group.

Model	Batch	Learn. rate	Im. width	mAP50
yolov8l	2	0.005	1600	0.972 ± 0.012
yolov8l	8	0.005	1280	0.952 ± 0.017
yolov8l	4	0.001	1600	0.927 ± 0.012
yolov8l	8	0.005	960	0.913 ± 0.021
yolov8m	8	0.001	1280	0.872 ± 0.005

The most reliable model (the first one in Table 2), was used to generate the external test set, trying to capture images with as many situations as possible (i.e. clear background, presence of dirt, quantity of eggshells, etc.), so that the general robustness of the model was estimated. In Table 3, the results on the internal test subset with egg-spiked and field samples are shown.

Given that both dilutions were typically adopted during the samples analysis, an average score of the following results should be considered. In Fig. 5, where there are all the confusion matrices obtained with inferences on both internal and external test set, the first two confusion matrices ((a)&(b)) are results with internal test set, one comparing detection results with labels made on scan images from KFM, the other with labels made on the same samples but with an optical microscope.

3.2. Validation of system robustness with external test set

After analyzing model performances on a controlled and balanced test set, it is needed to perform the same inferences steps but on a different test set, which should be not balanced, so that it reproduces the real-world classes frequencies, and ideal setups are not occurring. While the previous test session was needed to verify that the AI system is equally performing on all the available classes, this test session is useful to understand how robust the proposed system is on likely samples, since test set is extracted from naturally infected samples without cleaning or balancing processes.

Table 3
Evaluation metrics on test set with egg-spiked and field fecal samples.

Class	Sample Type	Count	TP	FP	FN	Precision	Recall	AP50	F1-Score
F. hepatica	Egg-spiked	1449	1396	235	53	0.856	0.963	0.967	0.906
C. daubneyi	Egg-spiked	1039	876	38	163	0.958	0.843	0.917	0.897
All	Egg-spiked	2488	2272	273	216	0.907	0.903	0.942	0.905
F. hepatica	Field	376	329	304	47	0.52	0.875	0.747	0.652
C. daubneyi	Field	858	521	20	337	0.963	0.607	0.805	0.745
All	Field	1234	850	324	384	0.741	0.741	0.776	0.741

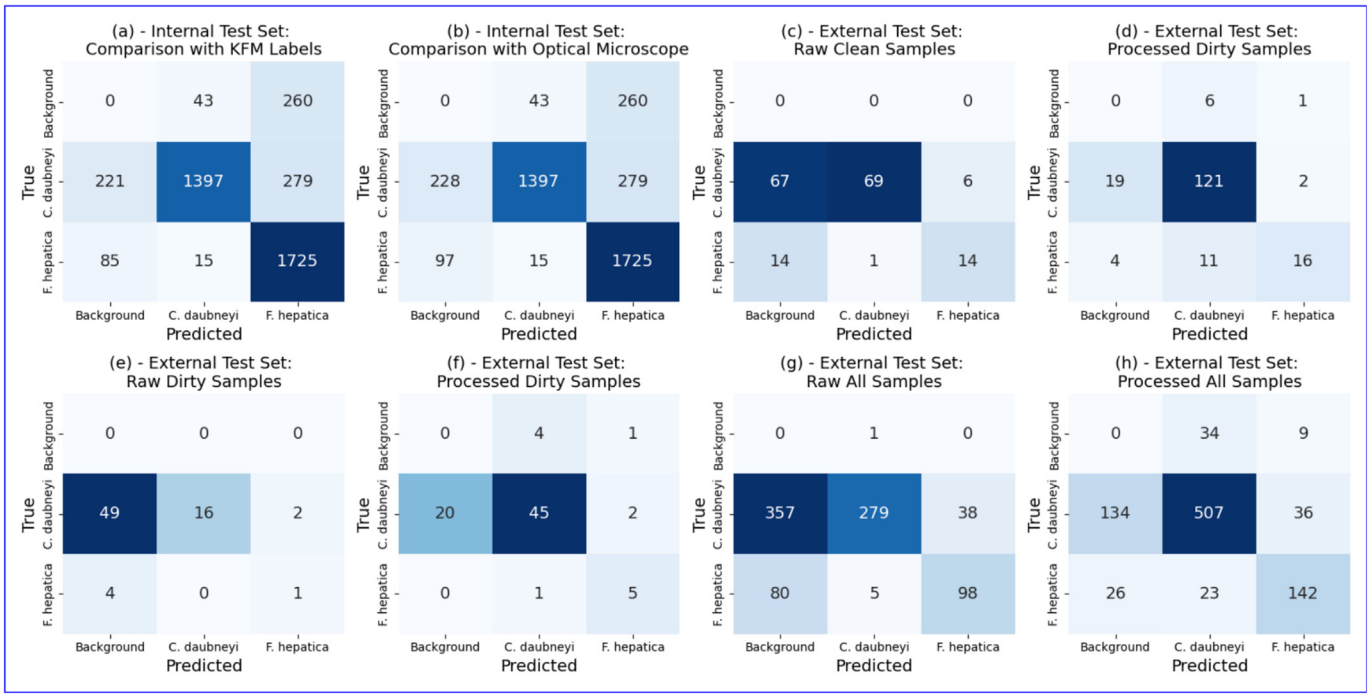

Fig. 5. Confusion matrices obtained after inferences made on internal and external test sets. The first two ((a)&(b)) are comparative results for the internal test set, while the others ((c)&(d), (e)&(f), (g)&(h)) are comparative results where couples are respectively results from raw data and pre-processed data. (a) compares detection results with ground-truth obtained from parasitologists by labeling KFM images, while (b) compares detection results with ground-truth obtained from the same sample, but labeled from an optical microscope. (c)&(d) are results from "clean" data, (e)&(f) from "dirty" data, (g)&(h) from all data.

For a complete and detailed analysis of the results, the 16 external test set scan sessions were classified with a value in the range from 1 to 5, where the higher value was associated with a dirtier floating chamber. In this experiment, given that samples are not forcefully extracted to obtain a minimum amount of elements per class, the egg classes are not balanced. Moreover, the dirtiness levels occurrences in this experiment follow, as expected, a Gaussian distribution.

The egg counts in the previous table were from a manual sample analysis using an optical microscope (OM). Therefore, the number of eggs for each class may not correspond to the real number of eggs, and this is due to KFM mechanical limitations. However, the aim of this study was to demonstrate that the detection system alone could compensate for possible mechanical deficiencies. Moreover, with the overlap-aware algorithm, the system was able to further reduce this difference, thereby providing a more reliable report.

In particular, Table 4 shows the results of the application of the AI workflow on the external test set, with a comparison between the workflow without and with processing steps, focusing on both the entire set and on subsets with specific levels of dirtiness. In Fig. 5, starting from (c), there are couples of confusion matrices comparing results on raw data with results on data processed with algorithms exposed in this work. The first couple is on "clean" data, the second on "dirty" data, the third on all the available test set.

As shown in Table 4 and in these confusion matrices, although the AP50 values were similar regardless of processing, the F1-Score increased significantly. This improvement occurred because the processing pipeline prevented the loss of several eggs, resulting in a higher recall value. Given the importance of counting the correct number of eggs, the F1-Score appears to be the best trade-off to recognize the most effective approach to detect parasite eggs.

All these results, however, consider the comparison between the predictions and the ground-truth (GT), but, as specified before, there could be a larger difference between the number of detected eggs and the real number counted with the optical microscope.

For this reason, in this case, the focus was not on the mean average precision of individual images, but on mean absolute error (MAE) between these two numbers for each class.

3.3. Optical microscope and KFM comparison results

The scatter plots in Fig. 6 show the paired comparisons, for each class, among the count made with OM, the one made with labels generated by domain experts such as parasitologists with scan images (GT), and the one made with the KFM system (the detection

Table 4
Results of the comparison between detections without and with processing steps.

Class	Dirtiness	Processed	Precision	Recall	AP50	F1-Score
F. hepatica	Low (1–2)	No	0.70	0.48	0.43	0.57
C. daubneyi	Low (1–2)	No	0.99	0.49	0.91	0.65
F. hepatica	High (4–5)	No	0.33	0.20	0.12	0.25
C. daubneyi	High (4–5)	No	1.00	0.24	0.95	0.39
F. hepatica	All	No	0.72	0.54	0.48	0.61
C. daubneyi	All	No	0.98	0.41	0.87	0.58
F. hepatica	Low (1–2)	Yes	0.84	0.52	0.52	0.64
C. daubneyi	Low (1–2)	Yes	0.88	0.85	0.86	0.86
F. hepatica	High (4–5)	Yes	0.62	0.83	0.53	0.71
C. daubneyi	High (4–5)	Yes	0.90	0.67	0.89	0.77
F. hepatica	All	Yes	0.76	0.74	0.62	0.75
C. daubneyi	All	Yes	0.90	0.75	0.86	0.82

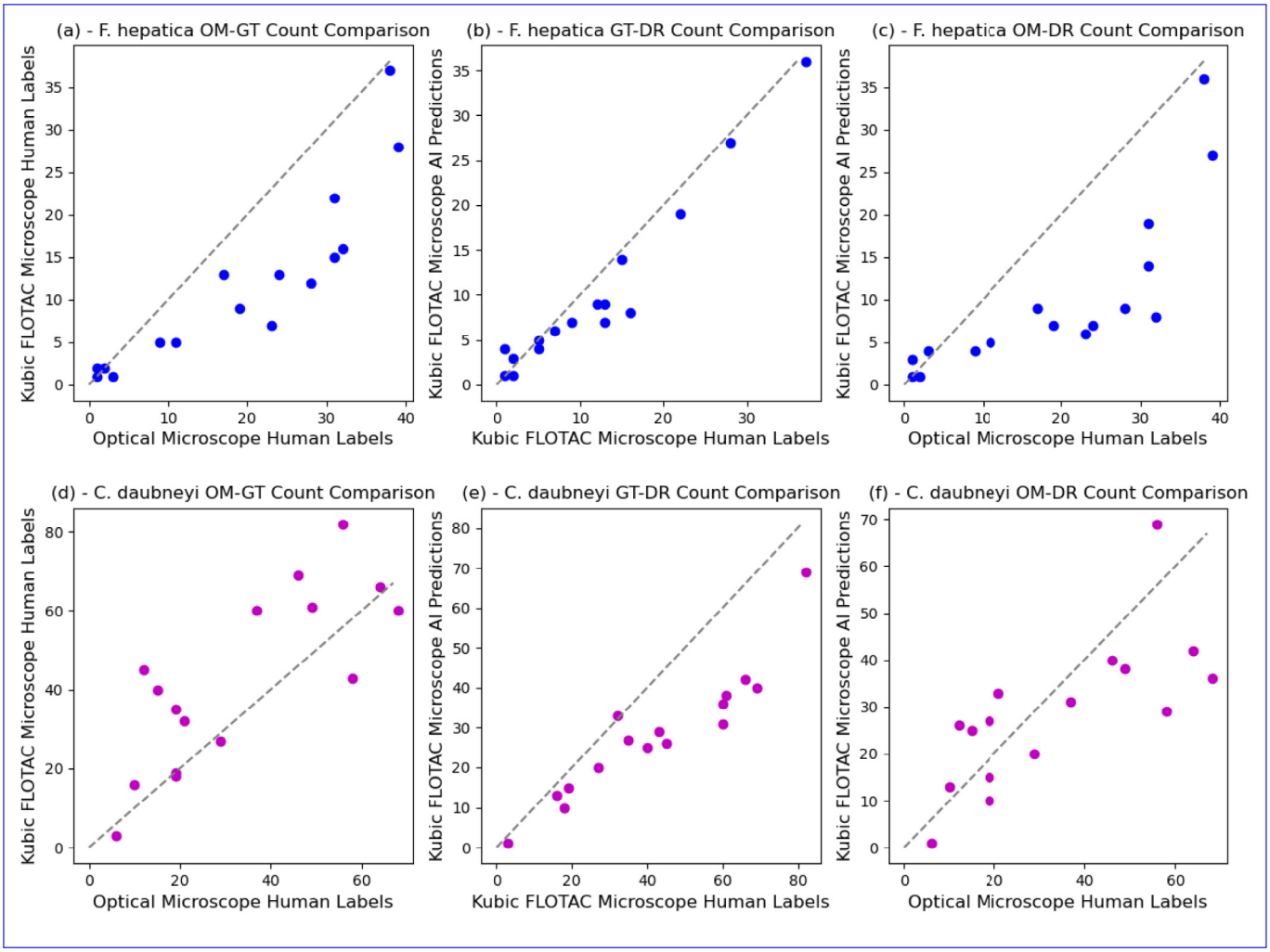

Fig. 6. Scatter plots of *F. hepatica* (blue) and *C. daubneyi* (purple) egg counts from OM (optical microscope, made by parasitologists), GT (ground-truth obtained with the KFM, made by parasitologists) and DR (detection results with the KFM, made by the AI system). Each point represents the comparison of how many eggs are in the analyzed scans according to two different points of view out of three.

results, or DR). In the plots, the closer the points are to the diagonal, the more similar the compared egg counts are. The count numbers obtained from the KFM system were the sum of TP and FP for each scan session of the external test set.

Considering the comparison between the labels provided by parasitologists with the KFM and the predictions made by the KFM AI system, which are represented in subfigures (b) and (e), the MAE on the count was approximately 2 eggs for *F. hepatica* and 14 for *C. daubneyi*. It is interesting to note that, at the same time, in the comparison between labels obtained with the optical microscope and AI predictions, Despite the higher number for the latter class, compared to the average scan sample population, the normalized MAE for *F. hepatica* was lower than for the other class. Indeed, confusion matrices and evaluation metrics, shown before, illustrate this performance loss on the *F. hepatica* class. However, considering the comparison with OM counts, the count error for the *F. hepatica* class became eight, but it almost kept the same value for the *C. daubneyi* class, meaning that there was no signifi-

cant loss between the scans performed by the OM and the one performed by KFM.

4. Discussion

The analysis of the results is divided into those obtained with the internal test set and those with the external test set, as they reflect different dataset characteristics. The internal test set consisted of a synthetic dataset split into two fecal sample preparations (egg-spiked and naturally infected), while the external test set consisted of field samples with class and concentration distributions representative of real-world conditions.

On the internal test set, the model achieved 96.7% AP50 for *F. hepatica* and an overall mAP50 of 94.2%. Performance was higher on images from the egg-spiked protocol, which were visually cleaner, than on naturally infected samples containing more debris.

When evaluated on the external test set, which contained only naturally infected samples, performance decreased to 77.6% mAP50. The highest AP50 in this scenario was obtained for *C. daubneyi* (80.5%). Differences between the true egg count and the labeled count were partly due to eggshells lost during manual scanning of KFM images because of focusing limitations in the version of the KFM used at the time of this study. These limitations have been addressed in subsequent hardware versions. The underestimation of labels was greater for *F. hepatica* than for *C. daubneyi*, suggesting that *F. hepatica* eggshells may be more frequently located at varying focal depths within the floating chamber. Further studies are ongoing to investigate the effect of runtime autofocusing on detection accuracy.

The computational resources available during this study allowed the use of models with higher complexity, prioritizing accuracy over latency. In practice, the inference time remained within a few seconds per sample. Future work will investigate models optimized for different trade-offs between accuracy and processing speed, particularly in combination with updated KFM hardware.

In addition to the DL model, the complete KFM pipeline includes image pre-processing steps to address lighting variations, overlapping fields of view, and color imbalances. These processing steps may contribute to maintaining detection performance in variable imaging conditions.

In contrast to this study, all the other papers never mention all the processing steps adopted to remedy the described problems, even the commercial ones. Therefore, none of them have been designed specifically for the recognition of similar classes of eggshells such as those analyzed.

Validation of additional parasite egg classes in the AI-KFM dataset is required before public commercial deployment. Some classes, such as *Eimeria spp.*, may require additional data collection and adjustments to the processing pipeline. Efforts are also ongoing to develop training strategies that reduce the manual labeling workload associated with a large number of detectable parasite egg classes in fecal samples.

5. Conclusions

In this study the complete KFM workflow was presented, from the preparation of Mini-FLOTAC apparatuses to the generation of final report to differentiate *F. hepatica* and *C. daubneyi* eggshells, which are similar and difficult to distinguish, even for experts. In this study the KFM system resulted very useful in performing this task autonomously, saving researchers time and avoiding labor-intensive activities. In addition to this, the KFM system, unlike most competitors, is a portable solution. Therefore, analysis can be performed on-field, significantly reducing the overall analysis time compared to other solutions.

Given the results from this study and after implementing the improvements identified during the evaluation process, the KFM can be considered a valid and reliable system to be adopted in parasitology laboratories for automatic analysis of these and other classes of parasite eggs available in the AI-KFM Dataset, which is still expanding with more and more labels and new classes.

CRediT authorship contribution statement

Ines Hammami: Formal analysis, Data curation.**Paola Vitiello**: Validation, Investigation, Formal analysis, Data curation.**Giuseppe Martone**: Writing – original draft, Validation, Data curation.**Biase Celano**: Software, Resources, Methodology.**Stefano Marrone**: Writing – review & editing, Supervision, Project administration.**Maria Paola Maurelli**: Writing – review & editing, Validation, Methodology, Formal analysis.**Laura Rinaldi**: Writing – review & editing, Supervision, Project administration.**Salvatore Capuozzo**: Writing – original draft, Visualization, Validation, Software, Methodology, Formal analysis, Data curation.**Carlo Sansone**: Supervision, Project administration, Funding acquisition.**Giuseppe Cringoli**: Supervision, Project administration, Methodology, Conceptualization.**Lavinia Ciuca**: Validation, Formal analysis.**Antonio Bosco**: Writing – review & editing, Validation, Methodology, Investigation.

Declaration of Competing Interest

The authors declare that they have no known competing financial interests or personal relationships that could have appeared to influence the work reported in this paper.

Acknowledgements

The project has received funding from the European Union's Horizon 2020 research and innovation program under grant agreement no. 101000365. This study was also supported by EU funding within the NextGenerationEU-MUR PNRR Extended Partnership initiative on Future Artificial Intelligence Research (Project No. PE00000013, FAIR).

References

Adrien, M.d.L., Schild, A.L., Marcolongo-Pereira, C., Fiss, L., Ruas, J.L., Grecco, F.B., Raffi, M.B., 2013. Acute fasciolosis in cattle in southern Brazil. Pesq. Vete. Bras. 33, 705–709. URL:https://doi.org/10.1007/s00436-012-3096-2.

AlDahoul, N., Karim, H.A., Momo, M.A., Escobar, F.I.F., Magallanes, V.A., Tan, M.J.T., 2023. Parasitic egg recognition using convolution and attention network. Scie. repo. 13, 14475. https://doi.org/10.1038/s41598-023-41711-3.

Amiri, S., Shemshadi, B., Shirali, S., Kheirandish, F., Fallahi, S., 2021. Accurate and rapid detection of Fasciola hepatica copro-DNA in sheep using loop-mediated isothermal amplification (LAMP) technique. Vete. medi. and scie. 7, 1316–1324. https://doi.org/10.1002/vms3.455/v2/response1.

Anuracpreeda, P., Tepsupornkul, K., Chawengkirttikul, R., 2017. Immunodiagnosis of paramphistomosis using monoclonal antibody-based sandwich ELISA for detection of Paramphistomum gracile circulating 16 kda antigen. Para. 144, 899–903. https://doi.org/10.1017/s003118201600264x.

Atcheson, E., Lagan, B., McCormick, R., Edgar, H., Hanna, R.E., Rutherford, N.H., McEvoy, A., Huson, K.M., Gordon, A., Aubry, A., et al., 2022. The effect of naturally acquired rumen fluke infection on animal health and production in dairy and beef cattle in the UK. Fron. in Vete. Scie. 9, 968753. https://doi.org/10.3389/fvets.2022.968753.

Barrett, D.C., 2013. Cattle review. UK Vet Live. 18. https://doi.org/10.12968/live.2013.18.3.75. 35–35. URL: https://doi.org/10.12968/live.2013.18.3.75.

Boelow, H., Krücken, J., Thomas, E., Mirams, G., von Samson-Himmelstjerna, G., 2022. Comparison of fecpakg2, a modified mini-flotac technique and combined sedimentation and flotation for the coproscopic examination of helminth eggs in horses. Para. & Vect. 15, 166. https://doi.org/10.1186/s13071-022-05266-y.

Bosco, A., Ciuca, L., Maurelli, M.P., Vitiello, P.,, G., Prada, J.M., Rinaldi, L., 2023. Comparison of Mini-FLOTAC, flukefinder® and sedimentation techniques for

detection and quantification of Fasciola hepatica and Calicophoron daubneyi eggs using spiked and naturally infected bovine faecal samples. Para. & vect. 16, 260. URL: https://doi.org/10.1186/s13071-023-05890-2, doi:10.1186/s13071-023-05890-2.

Cain, J., Wilson, D., Slusarewicz, P., 2024. An automated faecal egg count system for detection of Ascaridia galli ova in chickens. Jour. of Helm. 98, e49. https://doi.org/10.1017/s0022149x24000373.

Calvani, N.E.D., George, S.D., Windsor, P.A., Bush, R.D., Šlapeta, J., 2018. Comparison of early detection of Fasciola hepatica in experimentally infected merino sheep by real-time PCR, coproantigen ELISA and sedimentation. Vete. para. 251, 85–89. https://doi.org/10.1016/j.vetpar.2018.01.004.

Capuozzo, S., Marrone, S., Gravina, M., Cringoli, G., Rinaldi, L., Maurelli, M.P., Bosco, A., Orrù, G., Marcialis, G.L., Ghiani, L., et al., 2024. Automating parasite egg detection: insights from the first AI-KFM challenge. Fron. in Arti. Inte. 7, 1325219. https://doi.org/10.3389/frai.2024.1325219.

Capuozzo, S., Maurelli, M.P., Marrone, S., 2025. Trematodes ai-kfm dataset. URL: https://doi.org/10.17632/6bjcxw8dx2.1, doi:10.17632/6bjcxw8dx2.1. version 1.

Castle, T.G., Britton, L., Ripley, B., Ubelhor, E., Slusarewicz, P., 2024. Evaluation of Parasight All-in-One system for the automated enumeration of helminth ova in canine and feline feces. Para. & Vect. 17, 275. https://doi.org/10.1186/s13071-024-06351-0.

Charlier, J., De Meulemeester, L., Claerebout, E., Williams, D., Vercruysse, J., 2008. Qualitative and quantitative evaluation of coprological and serological techniques for the diagnosis of fasciolosis in cattle. Vete. para. 153, 44–51. https://doi.org/10.1016/j.vetpar.2008.01.035.

Charlier, J., Rinaldi, L., Musella, V., Ploeger, H.W., Chartier, C., Vineer, H.R., Hinney, B., von Samson-Himmelstjerna, G., Băcescu, B., Mickiewicz, M., et al., 2020. Initial assessment of the economic burden of major parasitic helminth infections to the ruminant livestock industry in Europe. Prev. Vete. Medi. 182, 105103. https://doi.org/10.1016/j.prevetmed.2020.105103.

Cringoli, G., Amadesi, A., Maurelli, M.P., Celano, B., Piantadosi, G., Bosco, A., Ciuca, L., Cesarelli, M., Bifulco, P., Montresor, A., et al., 2021. The Kubic FLOTAC microscope (KFM): a new compact digital microscope for helminth egg counts. Para. 148, 427–434. https://doi.org/10.1017/s003118202000219x.

Cringoli, G., Maurelli, M.P., Levecke, B., Bosco, A., Vercruysse, J., Utzinger, J., Rinaldi, L., 2017. The Mini-FLOTAC technique for the diagnosis of helminth and protozoan infections in humans and animals. Natu. prot. 12, 1723–1732. https://doi.org/10.1038/nprot.2017.067.

Cringoli, G., Rinaldi, L., Maurelli, M.P., Utzinger, J., 2010. FLOTAC: new multivalent techniques for qualitative and quantitative copromicroscopic diagnosis of parasites in animals and humans. Natu. prot. 5, 503–515. https://doi.org/10.1038/nprot.2009.235.

Cure-Bolt, N., Perez, F., Broadfield, L.A., Levecke, B., Hu, P., Oleynick, J., Beltrán, M., Ward, P., Stuyver, L., 2024. Artificial intelligence-based digital pathology for the detection and quantification of soil-transmitted helminths eggs. PLOS Negl. Trop. Dise. 18, e0012492. https://doi.org/10.1371/journal.pntd.0012492.

Dixon, R., Wescott, R., 1987. A fast and accurate fecal examination technique for diagnosis of Fasciola hepatica, in: ANNUAL MEETING OF THE AMERICAN ASSOCIATION OF VETERINARY PARASITOLOGISTS, Institution of Engineering and Technology (IET). p. 28. URL: doi: 10.1049/el:19870436, doi:10.1049/el:19870436.

Forstmaier, T., Knubben-Schweizer, G., Strube, C., Zablotski, Y., Wenzel, C., 2021. Rumen (Calicophoron/paramphistomum spp.) and liver flukes (Fasciola hepatica) in cattle—prevalence, distribution, and impact of management factors in Germany. Anim. 11, 2727. https://doi.org/10.3390/ani11092727.

Francis, E.K., Šlapeta, J., 2022. A new diagnostic approach to fast-track and increase the accessibility of gastrointestinal nematode identification from faeces: Fecpakg2 egg nemabiome metabarcoding. Inte. jour. for para. 52, 331–342. https://doi.org/10.1016/j.ijpara.2022.01.002.

Good, R., Scherbak, D., 2023. Fascioliasis, in: StatPearls [Internet]. StatPearls Publishing. doi:10.1093/oed/6337429720.

Gordon, D., Roberts, L., Lean, N., Zadoks, R., Sargison, N., Skuce, P., 2013. Identification of the rumen fluke, Calicophoron daubneyi, in GB livestock: possible implications for liver fluke diagnosis. Vete. para. 195, 65–71. https://doi.org/10.1016/j.vetpar.2013.01.014.

Hafizah, S.N., Izani, N.J.N., Najib, M.A., Wan-Nor-Amilah, W.A.W., 2023. Immunodiagnosis of Fascioliasis in Ruminants by ELISA Method: A Mini-Review. The Mala. jour. of medi. scie. MJMS 30, 25. https://doi.org/10.1089/mab.2023.0009.

Hanley, J., Garcia-Ara, A., Wapenaar, W., 2020. Cattle and sheep farmers' opinions on the provision and use of abattoir rejection data in the United Kingdom. Vete. Reco. 186. https://doi.org/10.1136/vr.105162. 217–217.

Hecker, A.S., Raulf, M.K., König, S., Knubben-Schweizer, G., Wenzel, C., May, K., Strube, C., 2024. In-herd prevalence of Fasciola hepatica and Calicophoron/paramphistomum spp. infections in German dairy cows with comparison of two coproscopical methods and establishment of real-time pyrosequencing for rumen fluke species differentiation. Vete. Para. 327, 110142. https://doi.org/10.1016/j.vetpar.2024.110142.

Howell, A., Baylis, M., Smith, R., Pinchbeck, G., Williams, D., 2015. Epidemiology and impact of Fasciola hepatica exposure in high-yielding dairy herds. Prev. vete. medi. 121, 41–48. https://doi.org/10.1016/j.prevetmed.2015.05.013.

Howell, A.K., Williams, D.J., 2020. The epidemiology and control of liver flukes in cattle and sheep. Vete. Clin. Food Anim. Prac. 36, 109–123. https://doi.org/10.1016/j.cvfa.2019.12.002.

Iglesias-Piñeiro, J., González-Warleta, M., Castro-Hermida, J.A., Córdoba, M., González-Lanza, C., Manga-González, Y., Mezo, M., 2016. Transmission of Calicophoron daubneyi and Fasciola hepatica in Galicia (Spain): Temporal follow-up in the intermediate and definitive hosts. Para. & Vect. 9, 1–14. https://doi.org/10.1186/s13071-016-1892-8.

Kahl, A., von Samson-Himmelstjerna, G., Helm, C.S., Hodgkinson, J., Williams, D., Weiher, W., Terhalle, W., Steuber, S., Krücken, J., 2023. Coproscopical diagnosis of patent fasciola hepatica infections in sheep–a comparison between standard sedimentation, flukefinder® and a combination of both. Vete. Para. 319, 109956. https://doi.org/10.1016/j.vetpar.2023.109956.

Kitvimonrat, A., Hongcharoen, N., Marukatat, S., Watcharabutsarakham, S., 2020. Automatic detection and characterization of parasite eggs using deep learning methods. In: in: 2020 17th International Conference on Electrical Engineering/Electronics, Computer, Telecommunications and Information Technology (ECTI-CON), IEEE. IEEE, pp. 153–156. https://doi.org/10.1109/ecti-con49241.2020.9158084.

Kumar, S., Arif, T., Ahamad, G., Chaudhary, A.A., Khan, S., Ali, M.A., 2023. An efficient and Effective Framework for Intestinal Parasite Egg Detection Using YOLOv5. Diag. 13, 2978. https://doi.org/10.21070/ups.1538. URL: https://doi.org/10.21070/ups.1538.

Kurnianto, H., Ramanoon, S.Z., Aziz, N.A.A., Indarjulianto, S., 2022. Prevalence, risk factors, and infection intensity of fasciolosis in dairy cattle in Boyolali, Indonesia. Vete. Worl. 15, 1438. https://doi.org/10.14202/vetworld.2022.1438-1448. URL: https://doi.org/10.14202/vetworld.2022.1438-1448.

Lalor, R., Cwiklinski, K., Calvani, N.E.D., Dorey, A., Hamon, S., Corrales, J.L., Dalton, J.P., De Marco Verissimo, C., 2021. Pathogenicity and virulence of the liver flukes Fasciola hepatica and Fasciola gigantica that cause the zoonosis Fasciolosis. Viru. 12, 2839–2867. https://doi.org/10.1080/21505594.2021.1996520.

Lee, J.J., Jung, B.K., Lim, H., Lee, M.Y., Choi, S.Y., Shin, E.H., Chai, J.Y., 2012. Comparative morphology of minute intestinal fluke eggs that can occur in human stools in the Republic of Korea. The Kore. jour. of para. 50, 207. https://doi.org/10.3347/kjp.2012.50.3.207.

Madsen, H., Stauffer, J.R., et al., 2022. Zoonotic trematode infections; their biology, intermediate hosts and control, in: Parasitic Helminths and Zoonoses-From Basic to Applied Research. IntechOpen. doi:10.5772/intechopen.102434.

Mage, C., Bourgne, H., Toullieu, J.M., Rondelaud, D., Dreyfuss, G., 2002. Fasciola hepatica and Paramphistomum daubneyi: changes in prevalences of natural infections in cattle and in Lymnaea truncatula from central France over the past 12 years. Vete. rese. 33, 439–447. https://doi.org/10.1051/vetres:2002030.

Mayo, P., Anantrasirichai, N., Chalidabhongse, T.H., Palasuwan, D., Achim, A., 2022. Detection of parasitic eggs from microscopy images and the emergence of a new dataset. arXi. prep. arXi. URL: doi: 10.2139/ssrn.5367031, doi:10.2139/ssrn.5367031.

McEvoy, A., O'Boyle, P., Ellis, S., Dalton, J.P., Parkinson, M., Keane, O.M., Machín, C., 2024. Comparison of traditional copromicroscopy with image analysis devices for detection of gastrointestinal nematode infection in sheep. Vete. Para. 329, 110216. https://doi.org/10.1016/j.vetpar.2024.110216.

Mitchell, G., 2002. Update on fasciolosis in cattle and sheep. In Prac. 24, 378–385. https://doi.org/10.1136/inpract.24.7.378.

Mitchell, G., Zadoks, R.N., Skuce, P.J., 2021. A universal approach to molecular identification of rumen fluke species across hosts, continents, and sample types. Fron. in Vete. Scie. 7, 605259. https://doi.org/10.3389/fvets.2020.605259.

Munita, M.P., Rea, R., Martinez-Ibeas, A.M., Byrne, N., Kennedy, A., Sekiya, M., Mulcahy, G., Sayers, R., 2019. Comparison of four commercially available ELISA kits for diagnosis of Fasciola hepatica in Irish cattle. BMC vete. rese. 15, 1–12. https://doi.org/10.1186/s12917-019-2160-x.

Nagamori, Y., Hall Sedlak, R., DeRosa, A., Pullins, A., Cree, T., Loenser, M., Larson, B.S., Smith, R.B., Goldstein, R., 2020. Evaluation of the VETSCAN IMAGYST: an in-clinic canine and feline fecal parasite detection system integrated with a deep learning algorithm. Para. & Vect. 13, 1–10. URL: https://doi.org/10.21203/rs.3.rs-52837/v1, doi:10.21203/rs.3.rs-52837/v1.

Nagamori, Y., Scimeca, R., Hall-Sedlak, R., Blagburn, B., Starkey, L.A., Bowman, D.D., Lucio-Forster, A., Little, S.E., Cree, T., Loenser, M., et al., 2024. Multicenter evaluation of the Vetscan Imagyst system using Ocus 40 and EasyScan One scanners to detect gastrointestinal parasites in feces of dogs and cats. Jour. of Vete. Diag. Inve. 36, 32–40. https://doi.org/10.1177/10406387231216185.

Naing, K.M., Boonsang, S., Chuwongin, S., Kittichai, V., Tongloy, T., Prommongkol, S., Dekumyoy, P., Watthanakulpanich, D., 2022. Automatic recognition of parasitic products in stool examination using object detection approach. Peer. Comp. Scie. 8, e1065. https://doi.org/10.7717/peerj-cs.1065.

Palasuwan, D., Naruenatthanaset, K., Kobchaisawat, T., Chalidabhongse, T.H., Nunthanasup, N., Boonpeng, K., Anantrasirichai, N., 2022. Parasitic egg detection and classification in microscopic images. IEEE Data. 5. https://doi.org/10.1007/s42979-023-02406-8.

Pedraza, A., Ruiz-Santaquiteria, J., Deniz, O., Bueno, G., 2022. Parasitic egg detection and classification with transformer-based architectures. In: in: 2022 IEEE International Conference on Image Processing (ICIP), IEEE. IEEE, pp. 4301–4305. https://doi.org/10.1109/icip46576.2022.9897846.

Pitié, F., Kokaram, A.C., Dahyot, R., 2007. Automated colour grading using colour distribution transfer. Comp. Visi. and Imag. Unde. 107, 123–137. https://doi.org/10.1016/j.cviu.2006.11.011.

Priddle, J., Mengersen, K., Swindells, D., Elliott, T., Ralph, C., 2025. Carcass weight, meat quality and economic impact of liver fluke infection on cattle. Vete. Para. Regi. Stud. and Repo. 58, 101195. https://doi.org/10.1016/j.vprsr.2025.101195.

Rajasekar, S.J.S., Jaswal, G., Perumal, V., Ravi, S., Dutt, V., 2023. Parasite. ai–An Automated Parasitic Egg Detection Model from Microscopic Images of Fecal Smears using Deep Learning Techniques. In: in: 2023 International Conference

on Advances in Computing, Communication and Applied Informatics (ACCAI), IEEE. IEEE, pp. 1–9. https://doi.org/10.1109/accai58221.2023.10200869.
Rashid, M.H., Stevenson, M.A., Waenga, S., Mirams, G., Campbell, A.J., Vaughan, J.L., Jabbar, A., 2018. Comparison of mcmaster and fecpak g2 methods for counting nematode eggs in the faeces of alpacas. Para. & vect. 11, 1–4. https://doi.org/10.1186/s13071-018-2861-1.
Ray, K., Shil, S., Saharia, S., Sarma, N., Karabasanavar, N.S., 2020. Detection and identification of parasite eggs from microscopic images of fecal samples, in: Computational Intelligence in Pattern Recognition: Proceedings of CIPR 2019, Springer. Springer Singapore. pp. 45–55. URL: doi: 10.1007/978-981-13-9042-5_5, doi:10.1007/978-981-13-9042-5_5.
Redmon, J., Divvala, S., Girshick, R., Farhadi, A., 2016. You only look once: Unified, real-time object detection, in. In: Proceedings of the IEEE conference on computer vision and pattern recognition. IEEE, pp. 779–788. https://doi.org/10.1109/cvpr.2016.91.
Reigate, C., Williams, H.W., Denwood, M.J., Morphew, R.M., Thomas, E.R., Brophy, P. M., 2021. Evaluation of two Fasciola hepatica faecal egg counting protocols in sheep and cattle. Vete. Para. 294, 109435. https://doi.org/10.1016/j.vetpar.2021.109435.
Rinaldi, L., Biggeri, A., Musella, V., De Waal, T., Hertzberg, H., Mavrot, F., Torgerson, P. R., Selemetas, N., Coll, T., Bosco, A., et al., 2015. Sheep and Fasciola hepatica in Europe: the GLOWORM experience. Geos. heal. 9, 309–317. https://doi.org/10.4081/gh.2015.353.
Ruiz-Santaquiteria, J., Pedraza, A., Vallez, N., Velasco, A., 2022. Parasitic egg detection with a deep learning ensemble. In: 2022 IEEE International Conference on Image Processing (ICIP), IEEE. IEEE, pp. 4283–4286. https://doi.org/10.1109/icip46576.2022.9897858.
Sabatini, G.A., de Almeida Borges, F., Claerebout, E., Gianechini, L.S., Höglund, J., Kaplan, R.M., Lopes, W.D.Z., Mitchell, S., Rinaldi, L., von Samson-Himmelstjerna, G., et al., 2023. Practical guide to the diagnostics of ruminant gastrointestinal nematodes, liver fluke and lungworm infection: interpretation and usability of results. Para. & Vect. 16, 58. https://doi.org/10.1186/s13071-023-05680-w.
Slusarewicz, P., Slusarewicz, J.H., Nielsen, M.K., 2021. Development and performance of an automated fecal egg count system for small ruminant strongylids. Vete. Para. 295, 109442. https://doi.org/10.1016/j.vetpar.2021.109442.
Soares, F.A., Suzuki, C.T.N., Sabadini, E., Falcão, A.X., de Oliveira Baccin, A., de Melo, L. C.V., Gomes, J.F., 2024. Laboratory validation of the automated diagnosis of intestinal parasites via fecal sample processing for the recovery of intestinal parasites through the dissolved air flotation technique. Para. & Vect. 17, 368. https://doi.org/10.1186/s13071-024-06434-y.
Steuer, A., Fritzler, J., Boggan, S., Daniel, I., Cowles, B., Penn, C., Goldstein, R., Lin, D., 2024. Validation of Vetscan Imagyst®, a diagnostic test utilizing an artificial intelligence deep learning algorithm, for detecting strongyles and parascaris spp. in equine fecal samples. Para. & Vect. 17, 465. https://doi.org/10.1186/s13071-024-06525-w.
Suwannaphong, T., Chavana, S., Tongsom, S., Palasuwan, D., Chalidabhongse, T.H., Anantrasirichai, N., 2023. Parasitic egg detection and classification in low-cost microscopic images using transfer learning. SN Comp. Scie. 5, 82.
Takeuchi-Storm, N., Denwood, M., Hansen, T.V.A., Halasa, T., Rattenborg, E., Boes, J., Enemark, H.L., Thamsborg, S.M., 2017. Farm-level risk factors for Fasciola hepatica infection in Danish dairy cattle as evaluated by two diagnostic methods. Para. & vect. 10, 1–11. https://doi.org/10.1186/s13071-017-2504-y.
Terven, J., Cordova-Esparza, D., 2023. A comprehensive review of YOLO: From YOLOv1 to YOLOv8 and beyond. 11, 677. https://doi.org/10.3390/machines11070677. arXi. prep. arXi..
Tyson, F., Dalesman, S., Brophy, P.M., Morphew, R.M., 2020. Novel equine faecal egg diagnostics: validation of the FECPAKG2. Anim. 10, 1254. https://doi.org/10.3390/ani10081254.
Viet, N.Q., ThanhTuyen, D.T., Hoang, T.H., 2019. Parasite worm egg automatic detection in microscopy stool image based on Faster R-CNN, in. In: Proceedings of the 3rd international conference on machine learning and soft computing. ACM, pp. 197–202. https://doi.org/10.1145/3310986.3311014.
Wang, Y., He, Z., Huang, S., Du, H., 2022. A Robust Ensemble Model for Parasitic Egg Detection And Classification. In: in: 2022 IEEE International Conference on Image Processing (ICIP), IEEE. Informa UK Limited, pp. 4258–4262. https://doi.org/10.1080/00401706.2000.10486016.
Wang, Z., Bovik, A.C., Sheikh, H.R., Simoncelli, E.P., 2004. Image quality assessment: from error visibility to structural similarity. IEEE tran. on imag. proc. 13, 600–612. https://doi.org/10.1109/tip.2003.819861.
Wang, Z., Liao, L., Huang, X., Tang, J., Lin, F., 2024. Evaluation of alarm notification of artificial intelligence in automated analyzer detection of parasites. Medi. 103, e39788. https://doi.org/10.1097/md.0000000000039788.
Ward, P., Levecke, B., Ajjampur, S., 2024. Harnessing artificial intelligence microscopy to improve diagnostics for soil-transmitted helminthiasis and schistosomiasis: a review of recent advances and future pathways. Curr. Opin. in Infe. Dise. 37, 376–384. https://doi.org/10.1097/qco.0000000000001048.
Ward, P.K., Roose, S., Ayana, M., Broadfield, L.A., Dahlberg, P., Kabatereine, N., Kazienga, A., Mekonnen, Z., Nabatte, B., Stuyver, L., et al., 2024b. A comprehensive evaluation of an artificial intelligence based digital pathology to monitor large-scale deworming programs against soil-transmitted helminths: a study protocol. Plos one 19, e0309816. URL: doi: 10.1101/2023.09.28.23296266, doi:10.1101/2023.09.28.23296266.
World Health Organization, 2021. Ending the neglect to attain the sustainable development goals. A road map for negl. trop. dise. 2030, 55. URL: https://doi.org/10.30875/9c96f135-en, doi:10.30875/9c96f135-en.
Xu, W., Zhai, Q., Liu, J., Xu, X., Hua, J., 2024. A lightweight deep-learning model for parasite egg detection in microscopy images. Para. & Vect. 17, 454. https://doi.org/10.1186/s13071-024-06503-2.